Nanoscale Optical Addressing of Valley Pseudospins through Transverse Optical Spin

Gong, Su Hyun; Komen, Irina; Alpeggiani, Filippo; Kuipers, L.

Important note
To cite this publication, please use the final published version (if applicable).
Please check the document version above.

Nanoscale Optical Addressing of Valley Pseudospins through Transverse Optical Spin

Su-Hyun Gong,*,§ Irina Komen,§ Filippo Alpeggiani, and L. Kuipers*

ACCESS | 📊 Metrics & More | 📰 Article Recommendations | 🆘 Supporting Information

ABSTRACT: Valley pseudospin has emerged as a good quantum number to encode information, analogous to spin in spintronics. Two-dimensional transition metal dichalcogenides (2D TMDCs) recently attracted enormous attention for their easy access to the valley pseudospin through valley-dependent optical transitions. Different ways have been reported to read out the valley pseudospin state. For practical applications, on-chip access to and manipulation of valley pseudospins is paramount, not only to read out but especially to initiate the valley pseudospin state. Here, we experimentally demonstrate the selective on-chip, optical near-field initiation of valley pseudospins at room temperature. We exploit a nanowire optical waveguide, such that the local transverse optical spin of its guided modes selectively excites a specific valley pseudospin. Furthermore, spin-momentum locking of the transverse optical spin enables us to flip valley pseudospins with the opposite propagation direction. Thus, we open up ways to realize integrated hybrid opto-valleytronic devices.

KEYWORDS: TMDC materials, WS$_2$, valleytronics, transverse optical spin, spin-momentum locking, ZnO nanowires
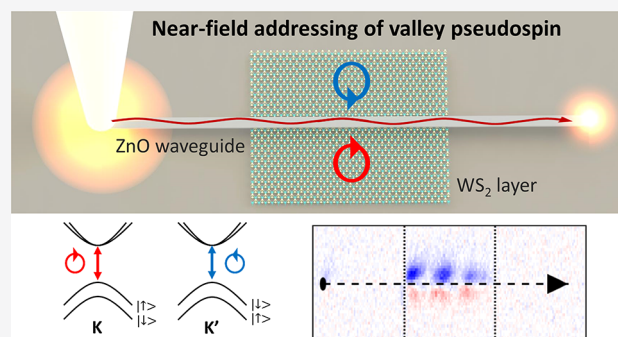
2D TMDCs possess direct bandgaps in the visible wavelength range at K and K′ in the Brillouin zone. Due to inversion symmetry breaking and spin−orbit coupling, a valley pseudospin and a spin can be attributed to the valleys of these materials.[1−3] Thus, an exciton has a valley and a spin-index, which is easily addressed using circularly polarized light.[9−12] These two valleys with their valley-dependent optical selection rules are schematically depicted in Figure 1b.

By now, it is well established that the longitudinal and transverse electric fields of propagating, guided modes yield transverse optical spin.[13,14] Since this transverse optical spin exhibits spin-momentum locking, the transverse spin flips sign upon reversal of the propagation direction of the guided light. This spin−orbit coupling of light has been used to steer light deterministically.[15−18] Furthermore, when transverse optical spin couples to an emitter with spin angular momentum, the interaction becomes chiral: the light−matter interaction depends on the propagation direction of the relevant light modes.[8,15,19−21] There have been several experimental demonstrations of spin-dependent directional emission from various materials as proof-of-principle experiments.[4−8] Here, the direction of emitted photons reflects the originating spin/valley state, which is thus optically read out. For realization of a chiral spin−photon interface, however, not only spin read-out but also spin addressing or transport via chiral spin−photon interaction should be demonstrated, but this still remains challenging. Here, we combine the valley pseudospins in TMDC layers with optical spin−orbit coupling near a

nanowire waveguide to demonstrate local propagation-dependent, selective valley addressing with near-field light. When combined with one of the ways shown for valley pseudospin read-out, real on-chip valleytronic devices with 2D TMDCs come one step closer.

Figure 1a depicts an overview of our experimental scheme. To launch guided modes, a laser beam is focused at the nanowire end. Subsequently, the propagating waveguide mode will have a transverse optical spin in its near-field, which will selectively excite specific valley pseudospins in the WS$_2$ layer. This local excitation will yield reradiating photons through spontaneous emission, depicted in Figure 1a by the red shading of the WS$_2$ on both sides of the nanowire. Some WS$_2$ emission will couple back into the guided mode of the nanowire, or into air or the glass (see Figure 1c). Please note that we collect the emitted light in the far-field on the glass side (see Figure S6 in the Supporting Information for a schematic representation of our experimental setup).
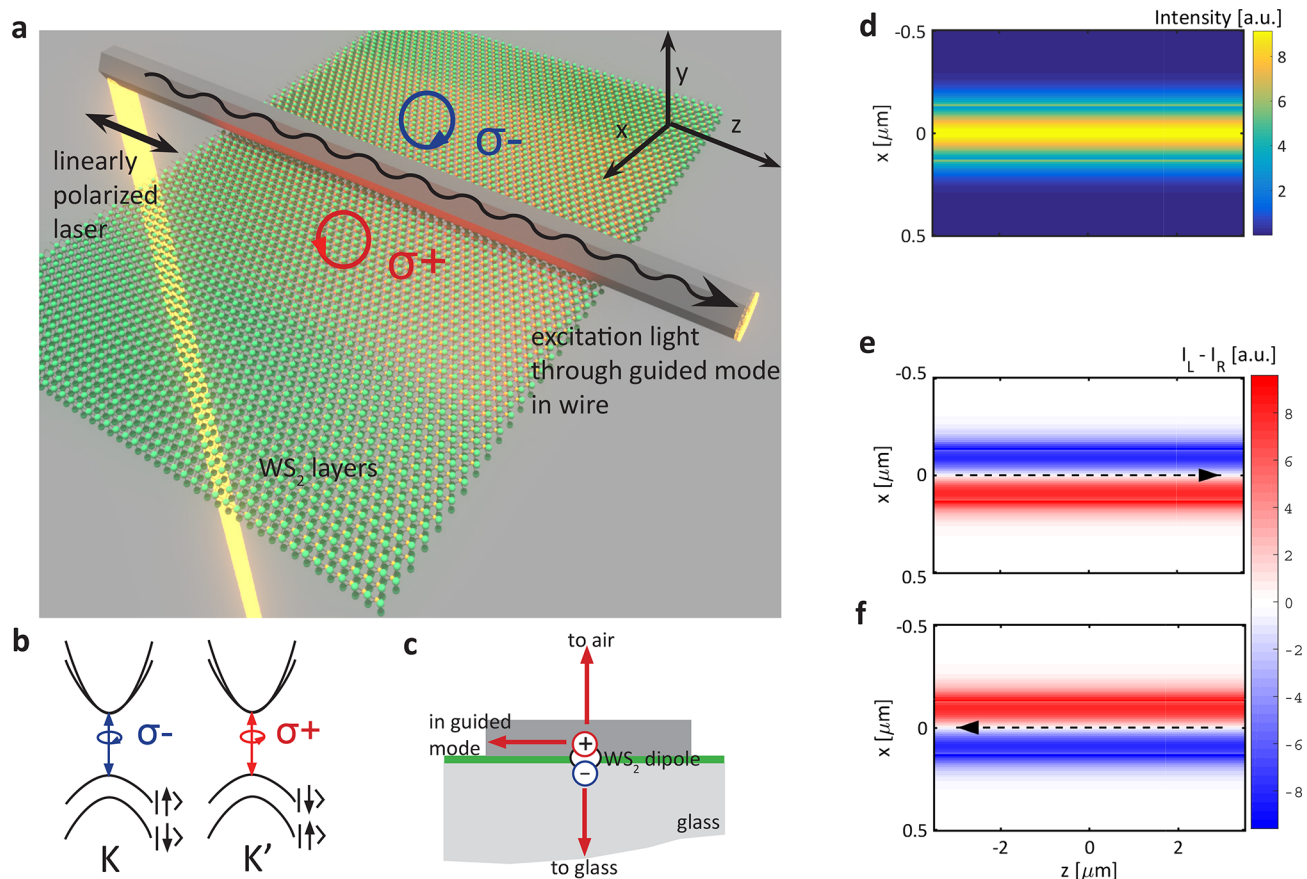
Figure 1d presents the simulated intensity distribution of the relevant guided optical mode for the plane between the
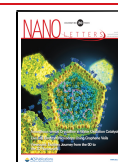
Figure 1. Schematic of the experiment: the transverse optical spin of guided modes in a nanowire addresses local valley pseudospins in WS$_2$ layers. (a) Sketch of the sample, with a nanowire on top of few-layer WS$_2$. A laser beam launches optical waveguide modes in the nanowire. Through their transverse optical spin, these modes locally excite the WS$_2$ valley pseudospins (lighting up in red). (b) Valley-dependent optical transition of WS$_2$. TMDC materials have two nonequivalent valleys at K and K′ symmetry points of the Brillouin zone. Excitons in specific valleys can be optically addressed with a specific circular polarization. (c) Emission from the addressed WS$_2$ excitons (depicted by a dipole) couples either back to the guided mode of the nanowire or into air or the glass substrate. We collect the emission into the glass. (d) Calculated intensity distribution of a guided ZnO nanowire mode in the plane of the WS$_2$, i.e., between the nanowire and the glass substrate. (e, f) Calculated spin density of this optical mode, propagating in the direction of the arrow. The blue and red colors indicate a clockwise and counterclockwise rotating electric field, respectively.

dielectric waveguide and the glass substrate, i.e., the plane where the WS$_2$ layers is located. The intensity is highest in the center of the nanowire and diminishes to the sides. A propagating mode in a waveguide has transverse optical spin momentum. Figure 1e depicts the calculated spin handedness of this optical mode using the non-normalized Stokes parameter $S_3 = I_L - I_R$ (the arrow depicts propagation direction). For $x < 0$, the handedness of the transverse optical spin is clockwise (blue color), whereas at the lower part of the picture near the nanowire, for $x > 0$, the handedness is anticlockwise (red color). Because of time-reversal symmetry, changing the propagation direction in the nanowire results in a reversal of all local rotation of electric fields (see Figure 1f). In short, the handedness of the local transverse optical spin is locked with the propagation direction of light.

In order to investigate valley polarization of addressed excitons directly through their free-space radiation, we use dielectric waveguides[22] for their advantages over the plasmonic waveguides that we used previously to investigate valley-dependent emission.[8] Both a metal and a dielectric waveguide will modify the radiation properties of excitons, such that much of the exciton emission couples to the waveguide again. This results in a weak free-space radiation signal. In addition, the

proximity of a nanowire will affect the polarization properties of the radiated field.[23] In practice, this means that emission from a perfect circular dipole would result in a reduced magnitude of S3 collected in the far-field. Our simulations show that dielectric waveguides have less influence than plasmonic waveguides on the intensity and especially on the polarization of the collected light (see Supporting Information I A and Figure S1 for details). Therefore, the lower coupling efficiency back to the dielectric waveguide modes as compared to a metal waveguide will enable us to observe direct radiation from the addressed excitons. Moreover, dielectric waveguides also have a lower propagation loss.

In this study, we have used chemically synthesized ZnO nanowires with a hexagonal cross-section, commercially available from the company ACS Materials. A single ZnO nanowire of radius 254 nm is located on top of a WS$_2$ flake with approximately five layers, as depicted in the optical image in Figure 2a (for an AFM image of the ZnO nanowire, see Supporting Information Figure S8a,b). At room temperature, the use of a multilayer WS$_2$ flake is preferred over a monolayer, since the multilayer exhibits a much higher degree of valley polarization due to the spin-layer locking effect.[24,25] Figure 2b shows the photoluminescence spectra of the flake used for
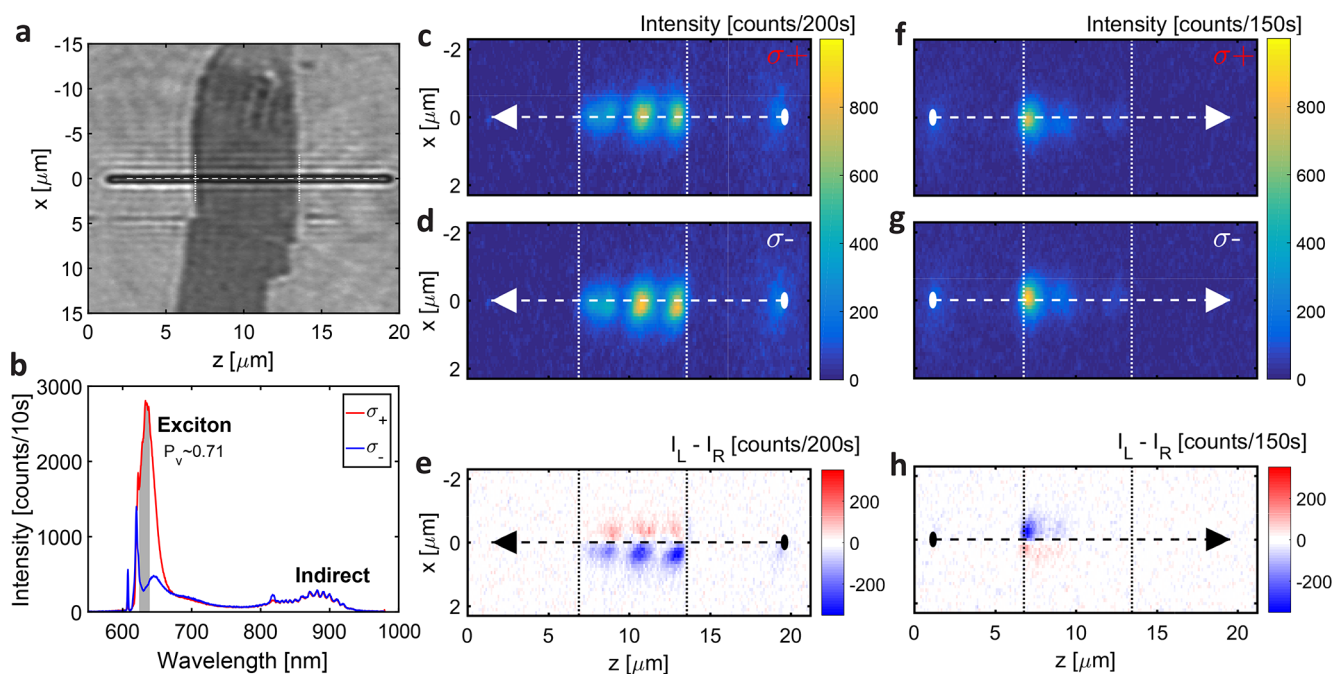
Figure 2. Photoluminescence images of valley-polarized excitons addressed by the near-field of waveguide modes. (a) Optical image of the WS$_2$ sample with the ZnO nanowire. The dotted lines coincide with the lines in parts c−h, indicating the center of the ZnO nanowire and the position of the WS$_2$ flake. (b) Photoluminescence of the WS$_2$ flake measured without the ZnO nanowire. The spectral position of the indirect bandgap emission indicates the number of WS$_2$ layers. The WS$_2$ is excited with σ_+ light, and from the difference in the σ_+ and σ_- emission, we determine a degree of valley polarization of 0.70. (c, f, d, g) Left (right) handed circularly polarized part of WS$_2$ photoluminescence (the arrow points in the propagation direction of the light in the nanowire). The emission intensity is not uniform along the nanowire but exhibits maxima and minima indicating mode interference. (e, h) By subtracting intensities in parts d and c, we determine the effective polarization handedness of the luminescence near the nanowire. The degree of circular polarization shows nonzero values at the positions of high intensity. In part e, the upper part of the picture for $x < 0$ has a positive handedness (red color) and the lower part for $x > 0$ has a negative handedness (blue color). In part h, these values are exactly flipped. We conclude that opposite WS$_2$ valley pseudospins are emitting at opposite sides of the nanowire. The handedness is as expected from the transverse optical spin of the ZnO nanowire modes (see Figure 1e,f). Therefore, opposite valley pseudospins are addressed selectively by the near-field of the ZnO nanowire modes.

Figure 2, measured without the ZnO nanowire. From the spectral position of the indirect bandgap, we determine the number of layers of the flake. We determine a degree of valley polarization of 0.70 from the difference in the σ_+ and σ_- emission, after exciting the WS$_2$ with σ_+ light.

We launch optical waveguide modes by shining a linearly polarized 595 nm laser light on the ZnO nanowire end. To investigate the WS$_2$ excitons excited via the transverse optical spin of the ZnO nanowire modes, free-space radiation of the excitons is collected and imaged on a CCD camera. Excitation light is filtered out, as is the light that is scattered from the nanowire end. An aperture at the Fourier plane of the optical setup reduces the numerical aperture of our detection system to 0.75 (for images with the full NA of 1.45, see Supporting Information II C and Figure S8). The degree of circular polarization of the emitted light is measured by using standard quarter waveplate projection (see Figure S6 in the Supporting Information for a schematic representation of our experimental setup).

Parts c, d, f, and g of Figure 2 present photoluminescence images at the exciton wavelength (620−630 nm, colored region in Figure 2b). Focusing laser light at the right end of the nanowire, i.e., launching the waveguide modes propagating in the direction of the arrow, left- and right-handed circularly polarized emission is selectively detected, as shown in Figure 2c and d, respectively. Bright emission can be clearly seen along the nanowire, coming only from the region of the WS$_2$ flake (see the dotted lines as in Figure 2a), indicating that all

emission comes from WS$_2$. The emission intensity is not constant along the nanowire, exhibiting maxima and minima, indicating mode interference (see below). We conclude that we have excited the WS$_2$ at both sides along the ZnO nanowire, using the near-field of the ZnO nanowire modes. When exciting the nanowire at the left end (Figure 2f,g) and thus changing the propagation direction of the light, left- and right-handed circularly polarized emission are again selectively detected, as shown in Figure 2f and g. Note the strength of the WS$_2$ photoluminescence, indicating the cleanliness of the interface between nanowire and WS$_2$.

To investigate the spatial distribution of the spin density even further, we subtract the intensity of the left-handed from the right-handed photoluminescence. By not normalizing the resulting signal, which would have yielded the normalized S3, we avoid noise, caused by low intensities, to dominate the figure, while staying as close as possible to the raw data. Note that the normalized S3, experimentally determined close to the nanowire (for $-1.5~\mu$m $< x < 1.5~\mu$m), has values between -0.3 and $+0.3$ (see Supporting Information Figure S5). Figure 2e demonstrates a handedness of the collected light at the three positions of maxima intensity. On the upper ($x > 0$) and lower ($x < 0$) side of the wire, the handedness has a positive (red color) and negative value (blue color), respectively. These opposite handednesses on either side of the waveguide are only visible in the presence of WS$_2$. Away from the waveguide, $I_L - I_R$ is roughly zero. When flipping the propagation direction in Figure 2h, we observe a similar effect. Now, however, the

handedness at each position has flipped sign: it is negative (blue) and positive (red) above and below the wire, respectively. When comparing this to the calculated transverse optical spin of the ZnO nanowire in Figure 1e,f, we note that the sign of the spin density matches for both propagation directions in the nanowire: the WS$_2$ excitons emit light from the two valleys with a sign corresponding to the local transverse optical spin of the nanowire. Where the transverse spin had a positive handedness, WS$_2$ excitons from the K valley emitted σ_+ light, and at negative handedness, excitons from the K′ valley emitted σ_-. As a control experiment, we collected emission from the indirect bandgap (see Supporting Information Figure S7), which did not show any nonzero spin density, as expected since this bandgap is not spin polarized. Therefore, we conclude that we have selectively and controllably addressed WS$_2$ excitons in their K and K′ valleys through the transverse spin of the ZnO nanowire modes.

To estimate the efficiency of the valley-selective excitation of our experimental system, we theoretically modeled the experimental situation. The first thing that catches the eye when comparing Figure 1d and our measured photoluminescence images in Figure 2c−h is the interference pattern. ZnO nanowires with a radius of 254 nm support several guided modes, in addition to leaky modes.[26] Using the finite element method, we identified the two relevant modes, whose combination of propagation constants explains the observed beat length (see Supporting Information I D). The interference pattern in the mode intensity is reflected in the spatial distribution of the exciton population.

In our model, we take into account both that we measure a diffraction-limited image of the exciton photoluminescence distribution and the 0.70 valley polarization of WS$_2$. Detailed information on the modeling is discussed in Supporting Information I E. Parts a and b of Figure 3 depict the modeled right-handed and left-handed circularly polarized emission distributions near a ZnO nanowire with radius 254 nm at the position of the WS$_2$ on the glass substrate, where the arrows indicate the propagation direction in the nanowire. The emission intensity is maximum around the center of the nanowire and is beating along the nanowire. Figure 3c represents the expected spin density around the nanowire, demonstrating how the beating phenomena affect the transverse optical spin. It is important to note that all different waveguide modes result in the optical spin with the same handedness in the region of evanescent fields (see Supporting Information I B and I C, Figure S2, and Figure S3). The mode beating results in a different intensity distribution along the nanowire, while having the same handedness and thus exciting the same WS$_2$ valleys regardless of their position. The normalized S3 close to the nanowire has values between −0.3 and +0.3.

It is clear that our simulation results in Figure 3 qualitatively reproduce our experimental results in Figure 2. To take a closer look while accounting for the beating pattern, crosscut profiles of Figure 2c,d and Figure 2f,g at the position of highest intensity are shown in Figure 4a and c. The position of the right-handed and left-handed parts of the WS$_2$ emission is not perfectly on the middle of the ZnO nanowire but is slightly shifted from the axis of symmetry. The same can be described qualitatively in simulation. In Figure 4b and d, crosscuts of the handedness are presented from Figures 2e,h and 3c. The plots are normalized for easy comparison. The normalized S3 in both experiment and simulation has values ranging from −0.3
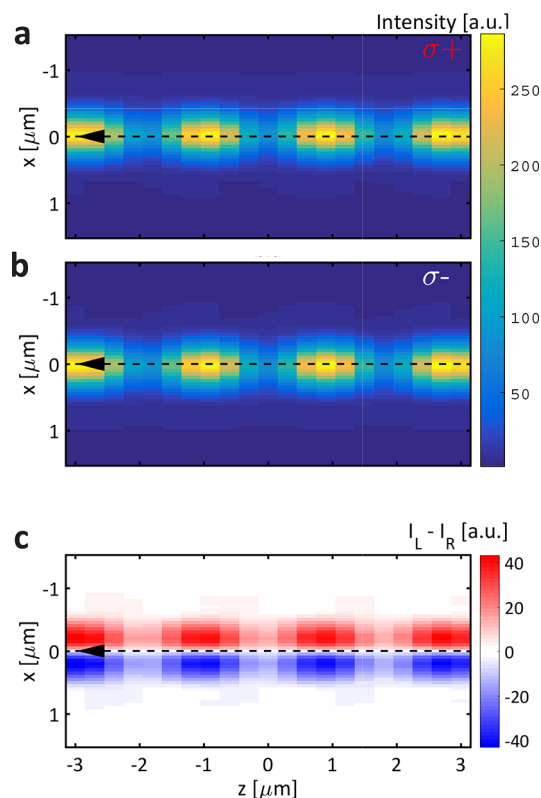
Figure 3. Simulation results of the polarization-dependent exciton emission near a ZnO nanowire. (a, b) Simulation of the photoluminescence of excitons with left (right) handed circular polarization near a 254 nm radius ZnO nanowire. Exploiting the reciprocity of light, we model in FDTD simulation the collection through a diffraction-limited system with an effective NA of 0.75, by focusing a circularly polarized Gaussian light source on a ZnO nanowire. The results are convolved with the calculated near-field intensity distribution of the mode beating pattern. (c) Degree of circular polarization, $I_L − I_R$, the non-normalized S3 of the exciton emission of the modes in the nanowire. For $x < 0$, the upper part of the nanowire, the handedness has negative values (red color), and in the lower part, it has positive values (blue color). The local sign of the handedness is the same as in the measurements in Figure 2e.

to +0.3 close to the waveguide, which is enough to distinguish the different polarization handedness at both sides of the nanowire already in the raw experimental data (see Supporting Information II A in Figure S5). No free parameters are required to achieve good quantitative agreement for data in both propagation directions. All of the relevant parameters (degree of valley polarization, size of the nanowire, relevant nanowire modes) are confirmed by independent measurements. The modes that are most likely to cause the experimentally measured beating pattern are selected based on the beating features in the data (see Supporting Information I D). Taking into account the valley polarization and the effect of diffraction-limited collection, we conclude that the ZnO nanowire guided modes excited the valley pseudospins in WS$_2$ with a near-unity selectivity. The lower measured value of S3 is caused mainly by the diffraction limit of our detection system and the presence of the nanowire (see the Supporting Information).

We demonstrated on-chip, local initiation of specific valley pseudospins in multilayer WS$_2$ with near-unity selectivity by exploiting the chiral photon−valley interaction mediated by
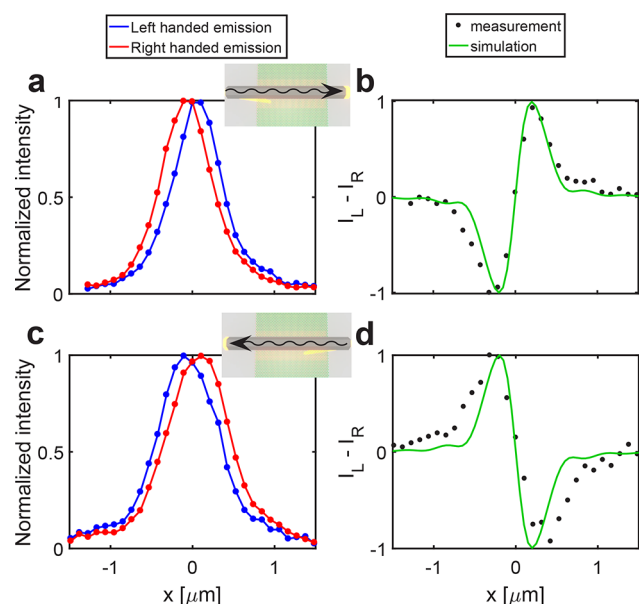
Figure 4. Normalized crosscuts of left- and right-handed WS$_2$ emission and the resulting spin density $I_L - I_R$ in both experiment and simulation. (a, c) Crosscuts of the experimentally measured left (in blue) and right (in red) handed part of the WS$_2$ emission shown in Figure 2b,c (e, f). The position of the emission is not perfectly in the middle of the ZnO nanowire (at $x = 0$) but is slightly shifted from the axis of symmetry. In part a, the right-handed emission (red color) is shifted to the left of the ZnO nanowire and the left-handed emission (blue color) is shifted to the right. Changing the propagation direction, indicated by the insets, flips the handedness of the emission in part c. (b, d) Crosscuts of $I_L - I_R$ from Figure 2e,h (black dots) compared with the calculated $I_L - I_R$ from Figure 3c (in red). The plots are normalized for easy comparison. The simulation results reproduce the experimental results very well qualitatively (for a quantitative comparison of the normalized S3, see Supporting Information Figure S5).

the transverse optical spin of propagating waveguide modes. The created valley polarization was quantified from the optical spin of the emission of the excitons collected in the far-field. As transverse optical spin and spin-momentum locking is a universal property of guided light, other waveguide materials can be chosen in the future to tailor the amount of far-field radiations to the desired device characteristics. This proof-of-concept adds addressability of valley pseudospin to the previously established on-chip optical read-out. Together, they can form the basis for on-chip integration of valleytronics and photonics.

ASSOCIATED CONTENT

Supporting Information

The Supporting Information is available free of charge at https://pubs.acs.org/doi/10.1021/acs.nanolett.0c01173.

> Simulation methods and complementary results; comparison between silver and ZnO nanowires, ZnO nanowire modes, and their interference; details on the simulation approach; experimental methods and complementary results; normalized S3 results, results at the wavelength of the indirect bandgap, and results with a full NA of the oil-immersion lens (PDF) Data acquired for this publication can be found at DOI: 10.4121/uuid:b45aadad-6687-40f2-8e60-fc1c2e583fdc

AUTHOR INFORMATION

Corresponding Authors
Su-Hyun Gong − *Kavli Institute of Nanoscience, Department of Quantum Nanoscience, Delft University of Technology, Delft, The Netherlands; Department of Physics, Korea University, Seoul, South Korea*; Email: shgong@korea.ac.kr

L. Kuipers − *Kavli Institute of Nanoscience, Department of Quantum Nanoscience, Delft University of Technology, Delft, The Netherlands;* ⓘ orcid.org/0000-0003-0556-8167; Email: L.Kuipers@tudelft.nl

Authors
Irina Komen − *Kavli Institute of Nanoscience, Department of Quantum Nanoscience, Delft University of Technology, Delft, The Netherlands;* ⓘ orcid.org/0000-0001-6805-090X

Filippo Alpeggiani − *Kavli Institute of Nanoscience, Department of Quantum Nanoscience, Delft University of Technology, Delft, The Netherlands*

Complete contact information is available at:
https://pubs.acs.org/10.1021/acs.nanolett.0c01173

Author Contributions
§S.-H.G., I.K.: These authors contributed equally.

Notes
The authors declare no competing financial interest.

REFERENCES

(1) Schaibley, J. R.; Yu, H.; Clark, G.; Rivera, P.; Ross, J. S.; Seyler, K. L.; Yao, W.; Xu, X. Valleytronics in 2D materials. *Nat. Rev. Mater.* **2016**, *1*, 16055.

(2) Mak, K. F.; Xiao, D.; Shan, J. Light-valley interactions in 2D semiconductors. *Nat. Photonics* **2018**, *12*, 451−460.

(3) Xu, X.; Yao, W.; Xiao, D.; Heinz, T. F. Spin and pseudospins in layered transition metal dichalcogenides. *Nat. Phys.* **2014**, *10*, 343.

(4) Krasnok, A.; Alù, A. Valley-Selective Response of Nanostructures Coupled to 2D Transition-Metal Dichalcogenides. *Appl. Sci.* **2018**, *8*, 1157.

(5) Sun, L.; Wang, C.-Y.; Krasnok, A.; Choi, J.; Shi, J.; Gomez-Diaz, J. S.; Zepeda, A.; Gwo, S.; Shih, C.-K.; Al, A.; Li, X. Separation of valley excitons in a MoS2 monolayer using a subwavelength asymmetric groove array. *Nat. Photonics* **2019**, *13*, 180−184.

(6) Hu, G.; Hong, X.; Wang, K.; Wu, J.; Xu, H.-X.; Zhao, W.; Liu, W.; Zhang, S.; Garcia-Vidal, F.; Wang, B.; Lu, P.; Qiu, C.-W. Coherent steering of nonlinear chiral valley photons with a synthetic Au-WS2 metasurface. *Nat. Photonics* **2019**, *13*, 467−472.

(7) Chervy, T.; Azzini, S.; Lorchat, E.; Wang, S.; Gorodetski, Y.; Hutchison, J. A.; Berciaud, S.; Ebbesen, T. W.; Genet, C. Room Temperature Chiral Coupling of Valley Excitons with Spin-Momentum Locked Surface Plasmons. *ACS Photonics* **2018**, *5*, 1281−1287.

(8) Gong, S.-H.; Alpeggiani, F.; Sciacca, B.; Garnett, E. C.; Kuipers, L. Nanoscale chiral valley-photon interface through optical spin-orbit coupling. *Science* **2018**, *359*, 443−447.

(9) Zeng, H.; Dai, J.; Yao, W.; Xiao, D.; Cui, X. Valley polarization in MoS2 monolayers by optical pumping. *Nat. Nanotechnol.* **2012**, *7*, 490.

(10) Mak, K. F.; He, K.; Shan, J.; Heinz, T. F. Control of valley polarization in monolayer MoS2 by optical helicity. *Nat. Nanotechnol.* **2012**, *7*, 494.

(11) Cao, T.; Wang, G.; Han, W.; Ye, H.; Zhu, C.; Shi, J.; Niu, Q.; Tan, P.; Wang, E.; Liu, B.; Feng, J. Valley-selective circular dichroism of monolayer molybdenum disulphide. *Nat. Commun.* **2012**, *3*, 887.

(12) Aivazian, G.; Gong, Z.; Jones, A. M.; Chu, R.-L.; Yan, J.; Mandrus, D. G.; Zhang, C.; Cobden, D.; Yao, W.; Xu, X. Magnetic control of valley pseudospin in monolayer WSe2. *Nat. Phys.* **2015**, *11*, 148.

(13) Aiello, A.; Banzer, P.; Neugebauer, M.; Leuchs, G. From transverse angular momentum to photonic wheels. *Nat. Photonics* **2015**, *9*, 789.

(14) Bliokh, K. Y.; Rodríguez-Fortuño, F. J.; Nori, F.; Zayats, A. V. Spin-orbit interactions of light. *Nat. Photonics* **2015**, *9*, 796.

(15) Lodahl, P.; Mahmoodian, S.; Stobbe, S.; Rauschenbeutel, A.; Schneeweiss, P.; Volz, J.; Pichler, H.; Zoller, P. Chiral quantum optics. *Nature* **2017**, *541*, 473.

(16) Rodríguez-Fortuño, F. J.; Marino, G.; Ginzburg, P.; O'Connor, D.; Martínez, A.; Wurtz, G. A.; Zayats, A. V. Near-Field Interference for the Unidirectional Excitation of Electromagnetic Guided Modes. *Science* **2013**, *340*, 328.

(17) Rodríguez-Fortuño, F. J.; Barber-Sanz, I.; Puerto, D.; Griol, A.; Martínez, A. Resolving Light Handedness with an on-Chip Silicon Microdisk. *ACS Photonics* **2014**, *1*, 762−767.

(18) O'Connor, D.; Ginzburg, P.; Rodríguez-Fortuño, F. J.; Wurtz, G. A.; Zayats, A. V. Spin-orbit coupling in surface plasmon scattering by nanostructures. *Nat. Commun.* **2014**, *5*, 5327.

(19) Mitsch, R.; Sayrin, C.; Albrecht, B.; Schneeweiss, P.; Rauschenbeutel, A. Quantum state-controlled directional spontaneous emission of photons into a nanophotonic waveguide. *Nat. Commun.* **2014**, *5*, 5713.

(20) Petersen, J.; Volz, J.; Rauschenbeutel, A. Chiral nanophotonic waveguide interface based on spin-orbit interaction of light. *Science* **2014**, *346*, 67−71.

(21) Coles, R. J.; Price, D. M.; Dixon, J. E.; Royall, B.; Clarke, E.; Kok, P.; Skolnick, M. S.; Fox, A. M.; Makhonin, M. N. Chirality of nanophotonic waveguide with embedded quantum emitter for unidirectional spin transfer. *Nat. Commun.* **2016**, *7*, 11183.

(22) Yan, R.; Gargas, D.; Yang, P. Nanowire photonics. *Nat. Photonics* **2009**, *3*, 569.

(23) Grzela, G.; Hourlier, D.; Gómez Rivas, J. Polarization-dependent light extinction in ensembles of polydisperse vertical semiconductor nanowires: A Mie scattering effective medium. *Phys. Rev. B: Condens. Matter Mater. Phys.* **2012**, *86*, No. 045305.

(24) Jones, A. M.; Yu, H.; Ross, J. S.; Klement, P.; Ghimire, N. J.; Yan, J.; Mandrus, D. G.; Yao, W.; Xu, X. Spin-layer locking effects in optical orientation of exciton spin in bilayer WSe2. *Nat. Phys.* **2014**, *10*, 130.

(25) Zhu, B.; Zeng, H.; Dai, J.; Gong, Z.; Cui, X. Anomalously robust valley polarization and valley coherence in bilayer WS2. *Proc. Natl. Acad. Sci. U. S. A.* **2014**, *111*, 11606−11611.

(26) Voss, T.; Svacha, G. T.; Mazur, E.; Müller, S.; Ronning, C.; Konjhodzic, D.; Marlow, F. High-Order Waveguide Modes in ZnO Nanowires. *Nano Lett.* **2007**, *7*, 3675−3680.